Article:
Ning, Y, Fielding, LA, Nutter, J et al. (3 more authors) (2019) Spatially-Controlled Occlusion of Polymer-Stabilized Gold Nanoparticles within ZnO. Angewandte Chemie International Edition, 131 (13). pp. 4346-4351. ISSN 1433-7851

https://doi.org/10.1002/ange.201814492

Spatially-Controlled Occlusion of Polymer-Stabilized Gold Nanoparticles within ZnO

Yin Ning,*[a] Lee A. Fielding,[b] John Nutter,[c] Alexander N. Kulak,[d] Fiona C. Meldrum,[d] and Steven P. Armes*[a]

(a) Department of Chemistry, University of Sheffield, Brook Hill, Sheffield, South Yorkshire S3 7HF, UK.

(b) The School of Materials, University of Manchester, Oxford Road, Manchester, M13 9PL, UK.

(c) Henry Royce Institute, Department of Materials Science and Engineering, University of Sheffield, Mappin Street, Sheffield, S1 3JD, UK.

(d) School of Chemistry, University of Leeds, Woodhouse Lane, Leeds, LS2 9JT, UK.

Abstract: In principle, incorporating nanoparticles into growing crystals offers an attractive and highly convenient route for the production of a wide range of novel nanocomposites. Herein we describe an efficient aqueous route that enables the *spatially-controlled* occlusion of gold nanoparticles (AuNPs) within ZnO crystals at up to 20 % by mass. Depending on the precise synthesis protocol, these AuNPs can be (i) solely located within a central region, (ii) uniformly distributed throughout the ZnO host crystal or (iii) confined to a surface layer. Remarkably, such efficient occlusion is mediated by a *non-ionic* water-soluble polymer, poly(glycerol monomethacrylate)$_{70}$ (G_{70}), which is chemically grafted to the AuNPs; pendent *cis*-diol side-groups on this steric stabilizer bind Zn^{2+} cations, which promotes nanoparticle interaction with the growing ZnO crystals. Finally, uniform occlusion of G_{70}-AuNPs within this inorganic host leads to faster UV-induced photodegradation of a model dye.

Biominerals provide many wonderful examples of the incorporation of water-soluble biomacromolecules within various inorganic crystals, such as bones, teeth and seashells.[1] However, incorporating *nanoparticles* into inorganic crystals is much more challenging.[2] This is because crystallization normally favors impurity expulsion, rather than occlusion.[3] Nevertheless, various inorganic nanoparticles (e.g. Pt, Au, Fe_3O_4, quantum dots, etc) have been encapsulated into zeolites,[4] metal–organic frameworks (MOFs),[5] and ionic crystals,[6] albeit typically at relatively low loadings. In related work, inorganic nanoparticles can also be incorporated into $CaCO_3$ (calcite)[7] or Cu_2O[8] respectively using a gel-trapping or confinement-based strategy.

There is a growing number of literature reports describing the occlusion of various *anionic* nanoparticles with appropriate surface functionality (such as carboxylate,[9] sulfonate[10] or sulfate groups[11]) within *single* crystals (e.g. calcite or ZnO). Such wholly synthetic systems provide a new approach for the preparation of new nanocomposite crystals, while enabling the convenient introduction of color,[7a, 7b] magnetism,[7b] fluorescence[6] or enhanced mechanical properties (e.g. hardness).[9b] However, good control over the *spatial distribution* of guest nanoparticles within growing host inorganic crystals has not yet been achieved.

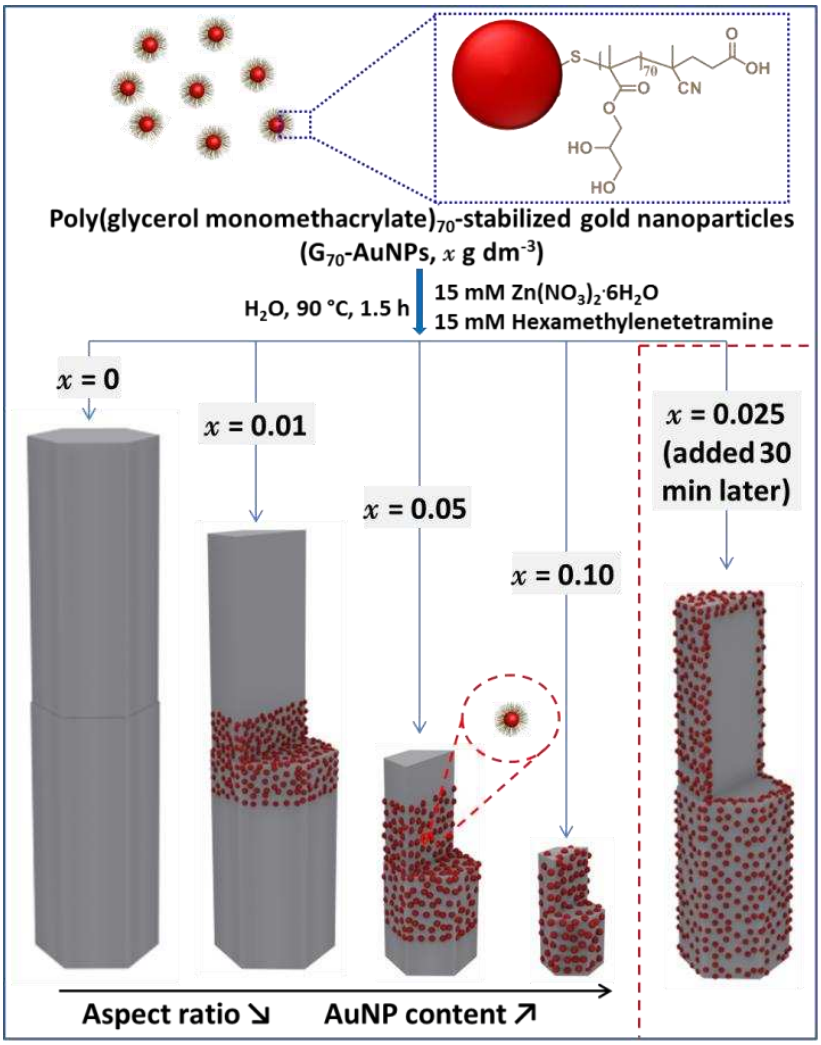

Scheme 1. Schematic representation of spatially-controlled occlusion of poly(glycerol monomethacrylate)$_{70}$-stabilized gold nanoparticles (G_{70}-AuNPs) within ZnO crystals. A twinned hexagonal rod-like ZnO crystal is obtained in the absence of any G_{70}-AuNPs (x = 0). In the presence of G_{70}-AuNPs, shorter twinned hexagonal ZnO rods are obtained. For x = 0.01 and 0.05, the G_{70}-AuNPs are preferentially located within the central region of the rods. In contrast, uniform spatial occlusion is achieved for x = 0.10. Finally, if the G_{70}-AuNP addition is delayed for 30 min when using x = 0.025, then only surface-confined occlusion is observed.

Herein we report efficient, spatially-controlled occlusion of *non-ionic* poly(glycerol monomethacrylate)$_{70}$-stabilized gold nanoparticles (G_{70}-AuNPs; see supporting information for further synthesis and characterization details, **Figures S1~S4**) within ZnO crystals generated in aqueous solution (**Scheme 1**). It is emphasized that this occlusion strategy differentiates our work from the many literature examples of Au/ZnO nanocomposites in which AuNPs are merely adsorbed at the surface of ZnO crystals.[12] Serendipitously, we found that G_{70}-AuNPs were efficiently incorporated within ZnO crystals generated by heating an aqueous solution containing $Zn(NO_3)_2{\cdot}6H_2O$ and hexamethylenetetramine at 90 °C for 1.5 h. In the absence of any G_{70}-AuNPs, twinned ZnO rods were obtained (**Figure 1a**). In the presence of 0.01 g dm^{-3} G_{70}-AuNPs (Au core diameter = 4.8 nm), nanoparticle occlusion was mainly confined to the central region of the ZnO rods, as indicated by the bracket shown in **Figure 1b**. [In addition, larger G_{70}-AuNPs (Au core diameter = 14 nm) were also prepared to aid nanoparticle imaging within the central region of the ZnO rods via SEM, see **Figure S5**]. Using a higher concentration of 4.8 nm G_{70}-AuNPs (0.05 g dm^{-3}) led to a larger central zone (**Figure 1c**, see brackets) and, when utilized at 0.075 g dm^{-3}, essentially all the G_{70}-AuNPs are more or less uniformly distributed throughout the ZnO crystals (**Figure S6**). At 0.10 g dm^{-3}, the G_{70}-AuNPs are uniformly distributed throughout the whole ZnO crystal (**Figure 1d**). The selected-area electron diffraction (SAED) pattern obtained for the ZnO control (see inset in **Figure 1a**) confirmed its single crystal nature. The same SAED pattern plus an additional ring of diffraction spots corresponding to AuNPs was observed for the G_{70}-Au(uniform)/ZnO nanocomposite crystals (see right inset in **Figure 1d**). Powder XRD studies confirmed that the ZnO particles always exhibited the wurtzite structure, whether they were prepared in the presence or absence of G_{70}-AuNPs (**Figure S7**).

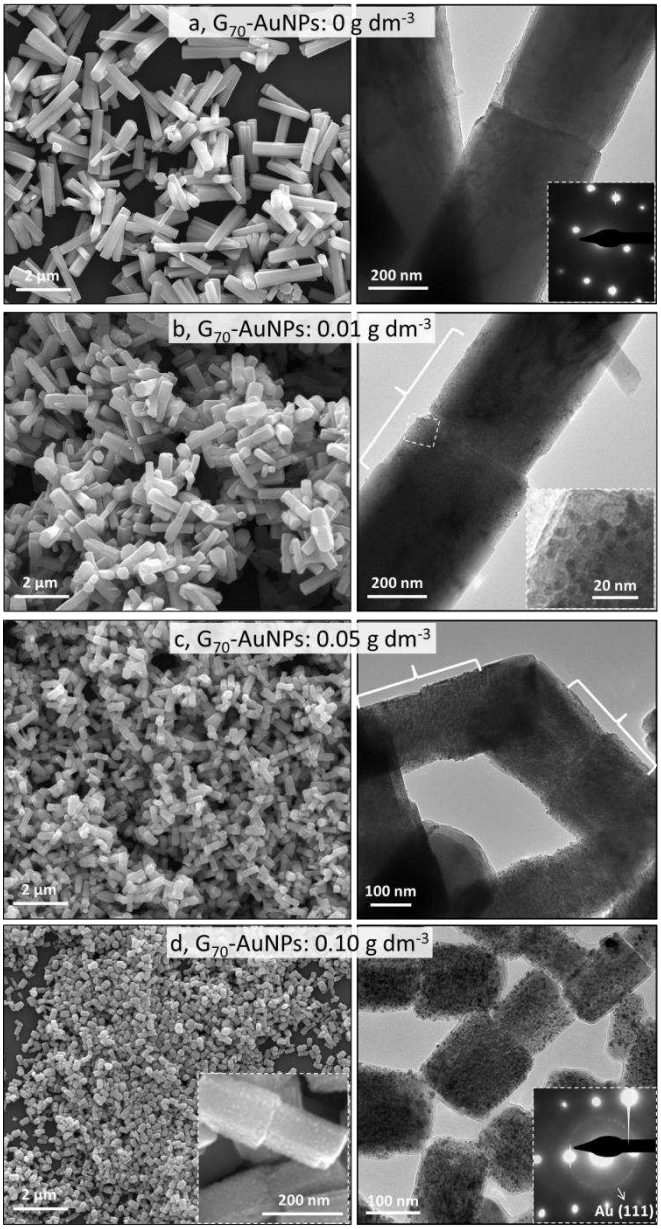

Figure 1. SEM images (left column) and TEM images (right column) obtained for ZnO crystals prepared in the presence of various concentrations (*x*) of G_{70}-AuNPs. (a), *x* = 0 g dm^{-3} G_{70}-AuNPs (pure ZnO control); (b) *x* = 0.01 g dm^{-3}; (c), *x* = 0.05 g dm^{-3}; (d), *x* = 0.10 g dm^{-3}; The insets in (a) and (d) in the TEM images represent selected-area electron diffraction (SAED) patterns recorded for each corresponding sample. The inset shown in (b) is a higher magnification TEM image of the indicated region. The left inset in (d) is a higher magnification SEM image showing ZnO rods surface-decorated with gold nanoparticles (see white dots). The right inset in (d) shows the corresponding SAED pattern, indicating the single crystal nature of these ZnO particles and also a ring of diffraction spots assigned to the Au (111) planes. The brackets shown in (b) and (c) indicate the spatial location of the AuNPs within the central region of the ZnO rods.

High-resolution TEM images recorded for ultramicrotomed G_{70}-Au/ZnO nanocomposite crystals embedded in epoxy resin confirmed that the G_{70}-AuNPs were incorporated within the host matrix, rather than merely being deposited on its surface (**Figure 2**). By imaging the cross-section parallel to the *c* axis of the ZnO crystals (**Figures 2a~2d**), G_{70}-AuNPs (which appear darker than the host crystal owing to their higher electron density) are clearly preferentially located within the central core of the ZnO rods when used at a relatively low concentration of 0.05 g dm^{-3} (denoted as G_{70}-Au(central)/ZnO, **Figures 2a~2c**). In contrast, a uniform distribution of AuNPs throughout the ZnO crystal was achieved at 0.10 g dm^{-3} (denoted as G_{70}-Au(uniform)/ZnO, **Figure 2d**). The spatial distribution of AuNPs was further examined by imaging cross-sections made perpendicular to the *c* axis of the G_{70}-Au/ZnO rods (**Figures 2e~2n**). In a control experiment, ultramicrotomed ZnO crystals prepared in the absence of any AuNPs exhibited the expected hexagonal shape (**Figure 2e**).[13] When using 0.10 g dm^{-3} G_{70}-AuNPs, G_{70}-AuNPs were homogeneously occluded throughout the ZnO rods (**Figure 2f**). At this point, we hypothesized that ZnO crystals might also be prepared in which G_{70}-AuNPs are solely located within a surface layer. This objective was achieved via delayed addition of the G_{70}-AuNPs during ZnO formation. Under such conditions, ultramicrotomed cross-sections indicate that G_{70}-AuNPs are mainly confined to a ~35 nm surface layer within the ZnO crystal (denoted as G_{70}-Au(surface)/ZnO), as shown in **Figures 2g** and **2h**. STEM-EDS elemental mapping for Au and Zn further confirms the surface-confined occlusion of AuNPs within the host ZnO crystals (see **Figures 2i-2l**).

Figures 2m and **2n** show high-resolution TEM images obtained for the G_{70}-Au(uniform)/ZnO sample, in which lattice fringes of Au and ZnO can be clearly observed. Importantly, no interfacial amorphous ZnO (or G_{70} layer) between the guest AuNP and host ZnO was observed, see **Figure 2n**. Further high magnification TEM images are shown in **Figures S8-S9**. Given the presence of the G_{70} stabilizer chains at the surface of the AuNPs, it is perhaps surprising that no distinct interfacial region is observed between the AuNPs and the ZnO matrix (**Figures 2n**). However, the surface density of the G_{70} chains on the AuNPs is calculated (see Supporting Information) to be approximately 0.54 chains nm^{-2}, which is relatively low.[14]

Hence ZnO crystal growth can penetrate within the G_{70} stabilizer layer, leading to intimate contact with the AuNP cores. This was confirmed by XPS studies, which indicate a charge transfer interaction between Au and ZnO (**Figure S10**). In this context, it is perhaps noteworthy that Asenath-Smith et al.[8b] also reported intimate contact between guest citrate-stabilized AuNPs and host Cu_2O crystals. Furthermore, Kulak et al.[10] did not observe any interfacial host-guest region for block copolymer-stabilized magnetite sols occluded within either calcite or ZnO.

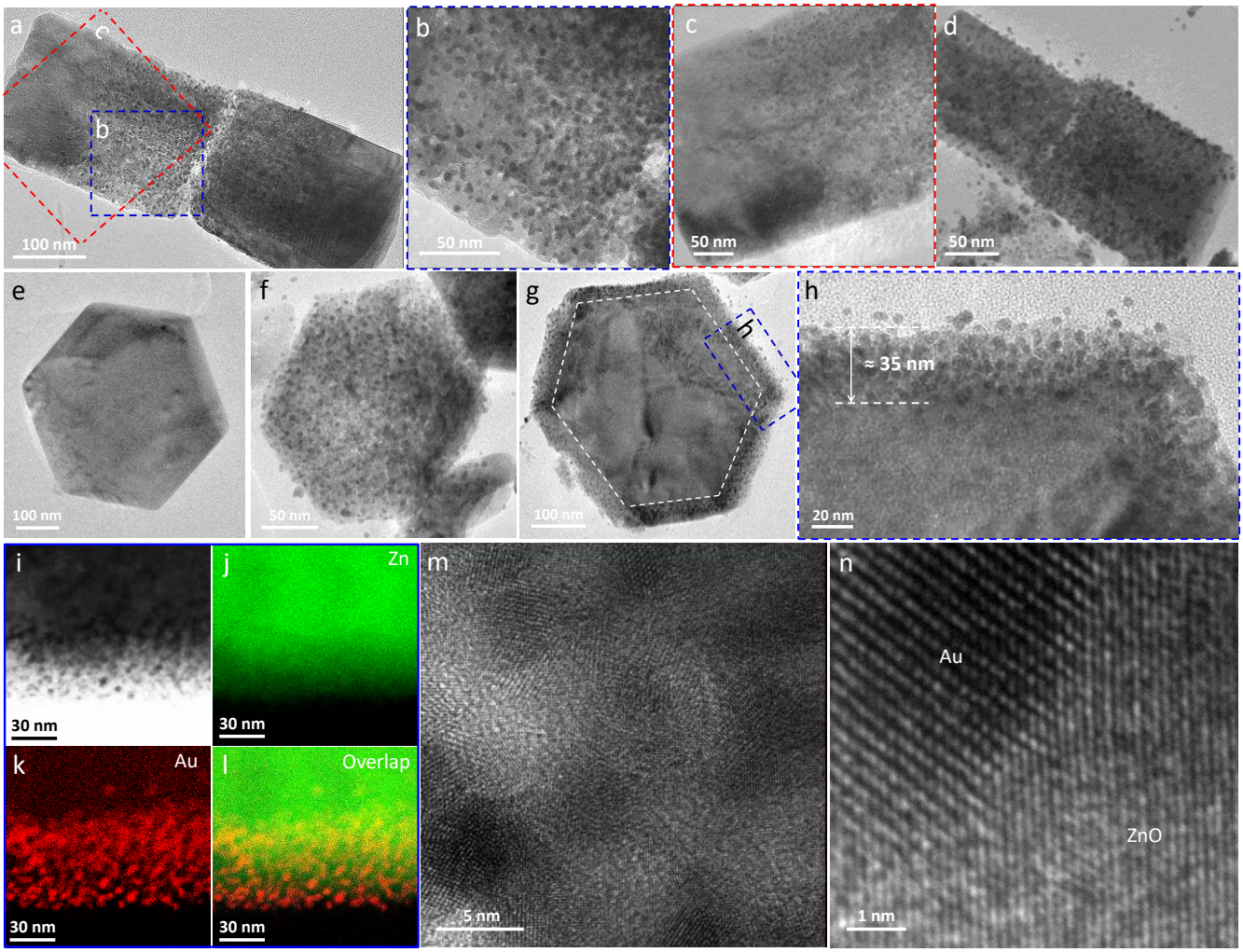

Figure 2. TEM images of ultramicrotomed cross-sections of G_{70}-Au/ZnO nanocomposite crystals with (a)~(d): parallel to the *c* axis and (e)~(n): perpendicular to the *c* axis. (a-c) 0.05 g dm^{-3} G_{70}-Au(central)/ZnO, with (b) and (c) representing magnified regions, as indicated in (a); (d) 0.10 g dm^{-3} G_{70}-Au(uniform)/ZnO. (e) ZnO control; (f) 0.10 g dm^{-3} G_{70}-Au(uniform)/ZnO; (g~h) G_{70}-Au(surface)/ZnO with G_{70}-AuNPs occluded within ZnO rod-like crystals in the form of a ~35 nm surface layer; (i)-(l) STEM-EDS elemental mapping of Au and Zn for G_{70}-Au(surface)/ZnO. (m) High resolution TEM images of uniformly-distributed AuNPs within ZnO and (n) the interface between the AuNPs and the ZnO host. The black dots shown in (m) indicate the AuNPs while in (n) it is clear that there is no amorphous ZnO or polymer layer at the interface between an individual AuNP and the ZnO lattice.

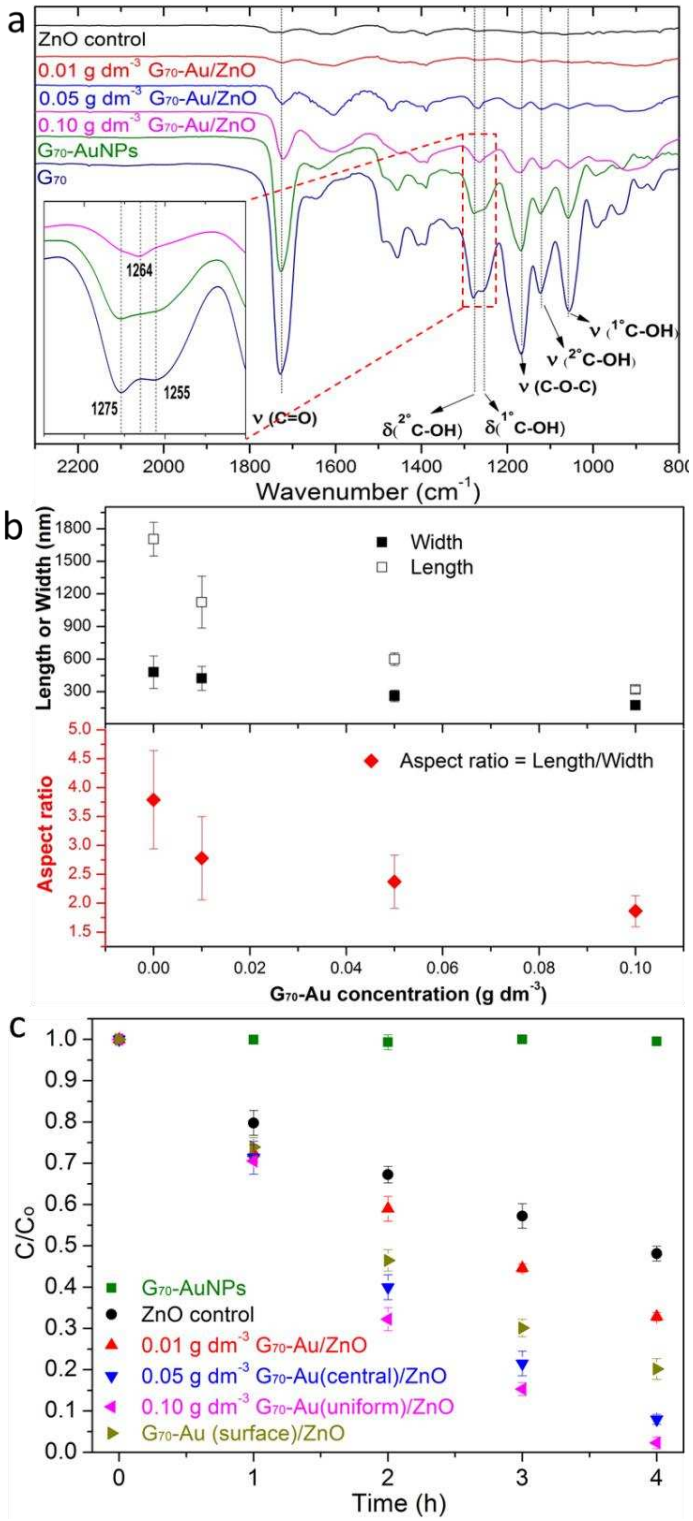

Figure 3. (a) FT-IR spectra recorded for three G_{70}-Au/ZnO nanocomposite crystals and three reference materials (ZnO crystals alone, G_{70} homopolymer and the G_{70}-AuNPs); (b) Length, width and aspect ratio of G_{70}-Au/ZnO versus G_{70}-AuNP concentration; (c) UV photocatalytic decomposition rates observed at 20 °C and pH 7 (6 W source, λ = 254 nm) for a model rhodamine B dye in the presence of three G_{70}-Au/ZnO nanocomposite crystals and two control samples.

The extent of G_{70}-AuNPs occlusion within ZnO increased when using higher G_{70}-AuNP concentrations, as determined by inductively-coupled plasma mass spectrometry (ICP-MS, **Table S1**). Remarkably, ZnO crystals containing up to 11.9 % gold by mass (or 19.9 % G_{70}-AuNPs by mass) can be prepared under uniform occlusion conditions, e.g. when using 0.10 g dm^{-3} G_{70}-AuNPs. Clearly, the G_{70} stabilizer chains play a key role in the interaction between the AuNPs and the growing host crystal. At first sight this seems rather counter-intuitive because the *non-ionic* nature of poly(glycerol monomethacrylate) might be expected to produce little or no interaction with the ZnO lattice. Indeed, previous reports suggest that *anionic* surface charge density is required for efficient interaction of copolymer nanoparticles within calcite or ZnO crystals.[9-11] The G_{70} chains used in this study contain a terminal carboxylic acid unit but further experiments confirm that such anionic end-groups are not actually required to achieve efficient occlusion within ZnO (**Figure S11**). So how do the G_{70}-AuNPs interact with the growing ZnO? Bearing in mind a report by Cölfen and co-workers on polyacrylamide interactions with ZnO crystals,[15] the most likely explanation involves chelation between the Zn^{2+} cations and the *cis*-diol groups on the non-ionic G_{70} stabilizer chains.[16] Experimental evidence for this complexation is provided by vibrational spectroscopy (**Figure 3a**). In FT-IR spectra recorded for G_{70}-AuNPs and G_{70} homopolymer, the absorption bands at 1255 cm^{-1} and 1275 cm^{-1} are assigned to the in-plane bending vibrations of primary and secondary C-OH, respectively.[17] These two bands merge to form a single new band at 1264 cm^{-1} for G_{70}-Au/ZnO nanocomposites, which supports the postulated chelation of Zn^{2+} cations by the G_{70} chains (see inset shown in **Figure 3a** and also **Figure S12** for the control experiment conducted in the presence of a stoichiometric amount of $Zn(NO_3)_2$).[18]

Compared to the ZnO control, the mean length and width of the G_{70}-Au/ZnO nanocomposite crystals are systematically reduced when grown in the presence of higher concentrations of G_{70}-AuNPs (**Figure 3b**). More specifically, the mean length is dramatically reduced relative to the mean width, resulting in a much lower aspect ratio for the anisotropic ZnO crystals. This indicates that G_{70}-AuNPs bind preferentially to the polar (0001) face relative to the six non-polar $(10\bar{1}0)$ faces, thereby retarding the crystal growth rate and producing less anisotropic ZnO rods (see Supporting Information for more detailed discussion).[9a] Preparation of 'core-shell' G_{70}-Au/ZnO crystals was also attempted but only G_{70}-Au(central)/ZnO structures were obtained. This is because the ZnO precursor cannot grow effectively on $(10\bar{1}0)$ faces after delayed addition but instead grows preferentially on the (0001) face (see **Scheme S1**). At a relatively low G_{70}-AuNP concentration (i.e. < 0.05 g dm^{-3}), nanoparticle occlusion is complete before ZnO crystallization has ceased, leading to G_{70}-AuNPs being confined within a central region. At higher G_{70}-AuNP concentrations, there are sufficient G_{70}-AuNPs present to become occluded throughout the host crystal, while ZnO growth is significantly retarded.

Finally, we briefly explored the photocatalytic properties of these Au/ZnO nanocomposite crystals with different spatial distribution of AuNPs. Preliminary data confirm that the rate of UV photodegradation of a model rhodamine B dye increases monotonically with their AuNP content (**Figure 3c**). More importantly, the catalytic efficiency obtained for G_{70}-Au(uniform)/ZnO significantly exceeds that of G_{70}-Au(surface)/ZnO, which suggests that uniform occlusion of G_{70}-AuNPs *within* ZnO promotes catalytic performance (see control experiments in **Figure S13** and further discussion in the Supporting Information).

In summary, we report an efficient, versatile and scalable route to incorporate sterically-stabilized gold nanoparticles within ZnO single crystals. This study provides the first example of nanoparticle occlusion within inorganic crystals with *well-controlled spatial distribution* as well as tunable extent of occlusion, which offers an unprecedented opportunity to elucidate synthesis-structure-property relationships. We show for the first time that a *non-ionic* polymer stabilizer can promote highly efficient nanoparticle occlusion into inorganic host crystals. This represents an important paradigm shift because almost all prior literature reports in this area utilize *anionic* polymers as steric stabilizers. We rationalize the occlusion mechanism in terms of Zn^{2+} complexation to the non-ionic stabilizer chains and demonstrate that incorporation of AuNPs into ZnO crystals enhances their photocatalytic performance. In principle, appropriate surface modification of various other metal nanoparticles should enable their efficient occlusion within ZnO (and perhaps other host crystals), thus providing access to a range of new functional nanocomposite materials that are likely to exhibit emergent properties. We intend to explore this concept in the near future.

Acknowledgements

The Overseas Study Program of Guangzhou Elite Project and EPSRC (EP/P005241/1) are acknowledged for PhD sponsorship and post-doctoral support of Y.N., respectively. We thank EPSRC for post-doctoral support (EP/J018589/1 and EP/K006290/1) and SPA acknowledges a five-year ERC Advanced Investigator grant (PISA 320372). We thank Prof. G. J. Leggett and Dr. D. Hammond for useful XPS discussion, Prof. B. Inkson and Dr. S. Tzokov for TEM assistance and Dr. C. **Hill for ultramicrotomy. We also thank the University of Sheffield Sorby Centre for HRTEM access.**

Keywords: spatially-controlled occlusion • metal/semiconductor nanocomposites • gold nanoparticles • ZnO • RAFT polymerization

References

[1] a) A. Berman, L. Addadi, S. Weiner, *Nature* **1988**, *331*, 546-548; b) A. Berman, L. Addadi, A. Kvick, L. Leiserowitz, M. Nelson, S. Weiner, *Science* **1990**, *250*, 664-667; c) H. A. Lowenstam, S. Weiner, *On biomineralization*, Oxford University Press: New York, 1989; d) S. Mann, D. D. Archibald, J. M. Didymus, T. Douglas, B. R. Heywood, F. C. Meldrum, N. J. Reeves, *Science* **1993**, *261*, 1286-1292; e) A. M. Belcher, X. H. Wu, R. J. Christensen, P. K. Hansma, G. D. Stucky, D. E. Morse, *Nature* **1996**, *381*, 56-58; f) S. Mann, *Oxford University Press: Oxford* **2001**; g) A.-W. Xu, Y. Ma, H. Cölfen, *J. Mater. Chem.* **2007**, *17*, 415-449; h) F. C. Meldrum, H. Cölfen, *Chem. Rev.* **2008**, *108*, 4332-4432; i) E. Weber, B. Pokroy, *CrystEngComm* **2015**, *17*, 5873-5883; j) F. Nudelman, N. A. Sommerdijk, *Angew. Chem. Int. Ed.* **2012**, *51*, 6582-6596.

[2] a) J. D. Pasteris, J. J. Freeman, B. Wopenka, K. Qi, Q. Ma, K. L. Wooley, *Astrobiology* **2006**, *6*, 625-643; b) C. H. Lu, L. M. Qi, H. L. Cong, X. Y. Wang, J. H. Yang, L. L. Yang, D. Y. Zhang, J. M. Ma, W. X. Cao, *Chem. Mater.* **2005**, *17*, 5218-5224; c) H. Li, H. L. Xin, D. A. Muller, L. A. Estroff, *Science* **2009**, *326*, 1244-1247; d) A. Hanisch, P. Yang, A. N. Kulak, L. A. Fielding, F. C. Meldrum, S. P. Armes, *Macromolecules* **2016**, *49*, 192-204.

[3] a) B. Kahr, R. W. Gurney, *Chem. Rev.* **2001**, *101*, 893-951; b) A. G. Shtukenberg, M. D. Ward, B. Kahr, *Chem. Rev.* **2017**, *117*, 14042-14090.

[4] N. Wang, Q. Sun, R. Bai, X. Li, G. Guo, J. Yu, *J. Am. Chem. Soc.* **2016**, *138*, 7484-7487.

[5] G. Lu, S. Li, Z. Guo, O. K. Farha, B. G. Hauser, X. Qi, Y. Wang, X. Wang, S. Han, X. Liu, *Nat. Chem.* **2012**, *4*, 310-316.

[6] a) T. Otto, M. Müller, P. Mundra, V. Lesnyak, H. V. Demir, N. Gaponik, A. Eychmüller, *Nano Lett.* **2012**, *12*, 5348-5354; b) M. Müller, M. Kaiser, G. M. Stachowski, U. Resch-Genger, N. Gaponik, A. Eychmüller, *Chem. Mater.* **2014**, *26*, 3231-3237.

[7] a) A. N. Kulak, P. Yang, Y.-Y. Kim, S. P. Armes, F. C. Meldrum, *Chem. Commun.* **2014**, *50*, 67-69; b) Y. Liu, W. Yuan, Y. Shi, X. Chen, Y. Wang, H. Chen, H. Li, *Angew. Chem. Int. Ed.* **2014**, *53*, 4127-4131; c) Y. Liu, H. Zang, L. Wang, W. Fu, W. Yuan, J. Wu, X. Jin, J. Han, C. Wu, Y. Wang, H. L. Xin, H. Chen, H. Li, *Chem. Mater.* **2016**, *28*, 7537-7543.

[8] a) A. E. DiCorato, E. Asenath-Smith, A. N. Kulak, F. C. Meldrum, L. A. Estroff, *Cryst. Growth Des.* **2016**, *16*, 6804-6811; b) E. Asenath-Smith, J. M. Noble, R. Hovden, A. M. Uhl, A. DiCorato, Y.-Y. Kim, A. N. Kulak, F. C. Meldrum, L. F. Kourkoutis, L. A. Estroff, *Chem. Mater.* **2017**, *29*, 555-563.

[9] a) R. Muñoz-Espí, Y. Qi, I. Lieberwirth, C. M. Gómez, G. Wegner, *Chem. Eur. J.* **2006**, *12*, 118-129; b) Y.-Y. Kim, K. Ganesan, P. Yang, A. N. Kulak, S. Borukhin, S. Pechook, L. Ribeiro, R. Kroeger, S. J. Eichhorn, S. P. Armes, B. Pokroy, F. C. Meldrum, *Nat. Mater.* **2011**, *10*, 890-896; c) K. Rae Cho, Y.-Y. Kim, P. Yang, W. Cai, H. Pan, A. N. Kulak, J. L. Lau, P. Kulshreshtha, S. P. Armes, F. C. Meldrum,

J. J. De Yoreo, *Nat. Commun.* **2016**, *7*, 10187; d) Y. Ning, L. A. Fielding, K. E. B. Doncom, N. J. W. Penfold, A. N. Kulak, H. Matsuoka, S. P. Armes, *ACS Macro Lett.* **2016**, *5*, 311-315; e) Y. Ning, D. J. Whitaker, C. J. Mable, M. J. Derry, N. J. W. Penfold, A. N. Kulak, D. C. Green, F. C. Meldrum, S. P. Armes, *Chem. Sci.* **2018**, *9*, 8396-8401; f) C. T. Hendley, L. A. Fielding, E. R. Jones, A. J. Ryan, S. P. Armes, L. A. Estroff, *J. Am. Chem. Soc.* **2018**, *140*, 7936-7945.

[10] a) A. N. Kulak, M. Semsarilar, Y.-Y. Kim, J. Ihli, L. A. Fielding, O. Cespedes, S. P. Armes, F. C. Meldrum, *Chem. Sci.* **2014**, *5*, 738-743; b) A. N. Kulak, R. Grimes, Y.-Y. Kim, M. Semsarilar, C. Anduix-Canto, O. Cespedes, S. P. Armes, F. C. Meldrum, *Chem. Mater.* **2016**, *28*, 7528-7536.

[11] a) Y. Ning, L. A. Fielding, T. S. Andrews, D. J. Growney, S. P. Armes, *Nanoscale* **2015**, *7*, 6691-6702; b) Y. Ning, L. A. Fielding, L. P. D. Ratcliffe, Y.-W. Wang, F. C. Meldrum, S. P. Armes, *J. Am. Chem. Soc.* **2016**, *138*, 11734-11742.

[12] a) W. He, H.-K. Kim, W. G. Wamer, D. Melka, J. H. Callahan, J.-J. Yin, *J. Am. Chem. Soc.* **2013**, *136*, 750-757; b) X. Liu, M.-H. Liu, Y.-C. Luo, C.-Y. Mou, S. D. Lin, H. Cheng, J.-M. Chen, J.-F. Lee, T.-S. Lin, *J. Am. Chem. Soc.* **2012**, *134*, 10251-10258; c) M. Murdoch, G. I. N. Waterhouse, M. A. Nadeem, J. B. Metson, M. A. Keane, R. F. Howe, J. Llorca, H. Idriss, *Nat. Chem.* **2011**, *3*, 489-492; d) J. Lee, H. S. Shim, M. Lee, J. K. Song, D. Lee, *J. Phys. Chem. Lett.* **2011**, *2*, 2840-2845; e) R. Jiang, B. Li, C. Fang, J. Wang, *Adv. Mater.* **2014**, *26*, 5274-5309; f) S. T. Kochuveedu, J. H. Oh, Y. R. Do, D. H. Kim, *Chem. Eur. J.* **2012**, *18*, 7467-7472; g) Y. H. Jang, S. Y. Yang, Y. J. Jang, C. Park, J. K. Kim, D. H. Kim, *Chem. Eur. J.* **2011**, *17*, 2068-2076.

[13] Z. L. Wang, *J. Phys. Condens. Matter* **2004**, *16*, R829.

[14] M. Liang, I. C. Lin, M. R. Whittaker, R. F. Minchin, M. J. Monteiro, I. Toth, *ACS Nano* **2010**, *4*, 403-413.

[15] Y. Peng, A.-W. Xu, B. Deng, M. Antonietti, H. Cölfen, *J. Phys. Chem.B* **2006**, *110*, 2988-2993.

[16] a) S. P. Kawatkar, D. A. Kuntz, R. J. Woods, D. R. Rose, G.-J. Boons, *J. Am. Chem. Soc.* **2006**, *128*, 8310-8319; b) B. Gyurcsik, L. Nagy, *Coord. Chem. Rev.* **2000**, *203*, 81-149; c) T. Ghoshal, S. Kar, S. Chaudhuri, *Cryst. Growth & Des.* **2007**, *7*, 136-141.

[17] G. Socrates, *Infrared and Raman characteristic group frequencies: tables and charts*, John Wiley & Sons, **2004**.

[18] N. J. Richards, D. G. Williams, *Carbohydr. Res.* **1970**, *12*, 409-420.